Conference on Modelling Fluid Flow (CMFF'25)
The 19th International Conference on Fluid Flow Technologies
Budapest, Hungary, August 26 - August 29, 2025

SUPERPOSITION OF SECONDARY FLOWS INSIDE ARTIFICIAL GEOMETRIES

Péter Friedrich[1], Benjamin Csippa[1], György Paál[1]

[1] Corresponding Author. Department of Hydrodynamic Systems, Faculty of Mechanical Engineering, Budapest University of Technology and Economics. Műegyetem rkp 3, H-1111 Budapest, Hungary, E-mail: pfriedrich@hds.bme.hu, bcsippa@hds.bme.hu, gypaal@hds.bme.hu

ABSTRACT

It has been hypothesised in the literature that secondary flows play a role in intracranial aneurysm formation. [1], [2] Complex flow fields develop inside the arteries, affected by several parameters. The irregular shape of the blood vessels means that the effects of the geometry features, such as bends or cross-section changes are superposed. The complexity of the flow-field is further increased by the pulsatile nature of the blood flow.

The aim of this research is to better understand the relationship between the geometry and the developed flow-field in the case of intracranial arteries. Artificial models were created, where the cross-section was assumed to be constant and circular. The models consisted of two bends with a straight section between them. During the study several parameters were changed in the model. These include the diameter of the pipe, the radii of the bends, the length of the straight section between the bends and finally the Reynolds number. All the parameter ranges were selected to correspond to those in real vessels. CFD simulations were carried out on the models using Ansys CFX.

The study is limited by the number of bends and the number of configurations. The simulations were steady state, the transient effects of the pulsatile flow were not studied. Future work can expand on this research by improving on these limitations or by increasing the number of bends.

Keywords: Aneurysm, haemodynamics, CFD, CFX, Secondary flow, Python

NOMENCLATURE

$\underline{Fr}$	[-]	frenet unit vector
$\underline{r}$	[-]	vector
p	[-]	arbitrary point in plane
r_c	[-]	centreline point in plane
$\underline{v}$	[m/s]	absolute velocity vector

Subscripts and Superscripts

n, b, t	normal, binormal, tangent components of the Frenet system
ax	axial velocity
sec	secondary velocity
rad	radial component
circ	circumferential velocity
x, y, z	axes

1. INTRODUCTION

Aneurysms are malformations of the blood vessel wall. Two shapes are known. One is the so-called fusiform aneurysm. These form on arteries in the abdomen, the artery grows out radially in all directions. The other form is the saccular aneurysm. These are typical inside the brain. A sac grows on the side of the blood vessel, and it is connected to it with a smaller neck section.

Aneurysms might not influence the patient and may go unnoticed for long times as they do not have distinctive symptoms. Their danger lies in the rupture of the sac. The rupture of the sac can lead to stroke. Stroke is still one of the leading sources of death in the world. With the use of modern digital medical imaging technologies getting more common more aneurysms are discovered. Once discovered, the aneurysm can be treated effectively. Modern treatments use flow diverter stents, which are a web-like structure made of biocompatible metal alloys. These are placed in the artery at the neck of the aneurysm using a catheter. Another common method is coiling, when a thin metal wire is coiled inside the sac itself. Both of these methods reduce the velocity of the blood inside the sac, so that it starts to coagulate, and then the aneurysm may disappear. Both methods are endovascular procedures, in contrast to older open surgery methods.

As aneurysms do not have distinctive symptoms they are often discovered by accident. Thus, their

formation and development are not well understood. There are several theories on the cause of the aneurysm initiation. The initiation and growth of the sac are complex biomechanical processes. It is also believed that elevated secondary flows also play a role in the formation of the aneurysm sac.

Secondary flows exist in many fields of fluid dynamics. Everywhere it means a flow which is perpendicular to the main flow direction. The importance of secondary flows varies among the various fields of fluid dynamics. For example, in river flows they are well studied. The secondary flows play an important role in the movement of sediment in the river. In the case of mixing vessels, the vertical circulation of the liquid is also a secondary flow. Secondary flows also develop inside pipe networks. Most often bends in the pipe induce the secondary flow, but valves and pumps can also do it. In most engineering cases secondary flows inside a pipe are disadvantageous. Therefore, most studies focus on their reduction or dissipation.

A mathematical approach was proposed by Dean back in 1927 [3]. He assumed a pipe with circular cross-section, constant diameter and bend radius. The work also assumed the radius of the bend to be large compared to the radius of the cross section of the pipe. It also assumed the Reynolds number to be small and the flow to be steady state.

Later research expanded on the work of Dean by focusing on pulsatile flows in curved pipes. The flow varied in a sinusoidal manner. It had similar limitations as the work by Dean. It was again assumed that the curvature of the pipe bend was bigger than the radius of the cross-section of the pipe. [4], [5]

Physiological curved geometries often are non-planar, and thus have torsion besides curvature. Researchers also investigated the effects of torsion on the secondary flows. Yamamoto et al. [6] investigated the effects of torsion numerically in a steady flow. Others demonstrated [7], [8], [9] in helical pipes that torsion causes asymmetric Dean vortices in the cross section of the pipe. The vortex in one half becomes bigger, while the other becomes smaller. Nijjari et al. [10] investigated pulsatile flows in a curved pipe bend with torsion with elastic walls.

The above-mentioned research only focused on helical vessels or singular pipe bends. The radius of the bend was constant, and larger than the radius of the cross-section. However, in physiological blood vessels several bends can occur in a short distance, which may influence the development of the secondary flows in the next bend downstream. The radius of the bend might not be constant throughout the bend.

This paper aims at investigating the superposition of bends within a short distance of each other and their effect on the developing secondary flows using computational fluid dynamics (CFD).

2. METHOD

In order to investigate the superposition of pipe bends and their effect on the secondary flows a simple geometry was created. The geometry had several parameters, and a parametric study was made.

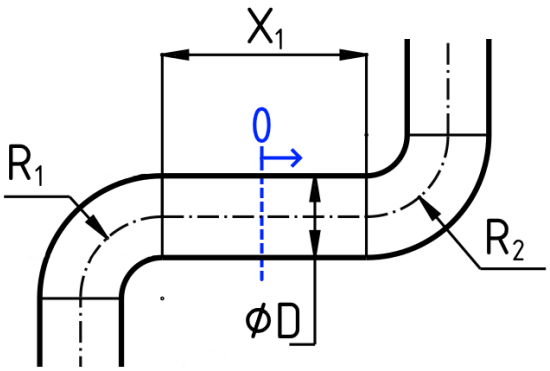

Figure 1. Parameters of the geometry, in blue the zero point for the post-processing coordinate-system

The geometry is a pipe with a circular cross-section and consists of straight and curved sections. The curved sections were each a 90° bend in opposite directions. Between the pipe bends there was a straight section. Before the first bend and after the second bend straight sections were made with 20 diameters in length. This was done to ensure a fully developed flow to arrive at the first bend, and to observe the dissipation of the secondary flows after the second bend. The geometry was created using FreeCAD 0.21.2 via the Python API. The geometry had the diameter of the pipe D, the radii of the bends R_1, R_2 and the length of the straight section between the bends x_1 as parameters. These can also be seen in Figure 1. The geometries were exported as an open surface mesh in the .stl format.

Meshing of the geometries was carried out with the Vascular Modelling Toolkit (VMTK) Python package. The mesh had an element size of 0.3 *mm* with tetrahedral elements. The inflation on the wall consisted of 8 layers, with a growth ratio of 1.25. The mesh settings were identical for all the cases. For the CFD simulations Ansys CFX 23R2 was used. The simulations were steady state. The fluid chosen was water. The inlet was set up as a velocity inlet, with a parabolic velocity profile. The mean velocity of the profile was calculated from the Reynolds-number prescribed for the given simulation. As the possible maximum Reynolds-number in the parameter set was 800, no turbulence model was used. The outlet was set as an opening with 0 *Pa*. The walls were rigid and set as non-slip walls.

The parameters of the study were the diameter of the pipe (D), the radii of the pipe bends (R), the length of the straight section between the bends (x_1) and the Reynolds-number (Re). The radii for the pipe

bends were the same for a given case, so the geometry is centrally symmetrical. They were defined using the R/D ratio. The value of x_1 was also made dimensionless using the diameter of the pipe. The ranges were selected, based on data from real arteries used in previous research. The range and increments of the parameters can be seen in Table 1. By multiplying the number of possible values for each the total number of cases is 990.

Table 1. Ranges and increments of the parameters

Parameter	Minimum	Maximum	Increment
D [mm]	3	5	1
R/D [-]	1	10	1
x_1 [-]	0	10	1
Re [-]	100	800	350

The parametric study was run using the Dakota open-source package. It managed the running of the cases, including modifying the scripts and commands necessary for running the simulations and post-processing. It also managed running the cases parallelly, thus greatly reducing the time required for running all the cases.

3. POST-PROCESSING

The post-processing was carried out using Paraview 5.10.1 and custom in-house built Python scripts. The post-processing focuses on the decomposition of the velocity field into secondary components. The decomposition is done using Frenet frames along the centreline of the geometry. A clear understanding of the Frenet frames is essential.

For each geometry a centreline can be calculated. Along this centreline, at any given point an orthogonal coordinate-system can be defined. In case of a Frenet-system each of the three axes point to a specified direction. The Frenet tangent vector $\underline{Fr_t}$ is parallel to the tangent of the centreline at that point. The Frenet normal vector $\underline{Fr_n}$ is perpendicular to the Frenet tangent vector, and points towards the centre of the tangent circle of the centreline. The third axis is the Frenet binormal vector $\underline{Fr_b}$ and is perpendicular to the other two axes. All of them are unit vectors. By using the Frenet normal and binormal vectors a plane can be defined. The geometry can be sliced with this plane. All further calculations were carried out on these slices.

The centreline was defined according to the geometrical parameters. The centreline was sampled at 0.1 mm intervals. A Python script calculated the Frenet unit vectors at each point.

The velocity field can be decomposed into an axial component and a secondary component. The first are parallel to the centreline, while the second are perpendicular to it, and lies in the plane of the slice. The axial component is calculated first using the Frenet tangent vector as can be seen in Eq. (1). Using Eq. (2) the secondary component can be calculated by subtracting the axial component, $\underline{v}_{ax}$, from the velocity vector $\underline{v}$.

$$\underline{v}_{ax} = (\underline{v} \cdot \underline{Fr_t}) \cdot \underline{Fr_t} \tag{1}$$

$$\underline{v}_{sec} = \underline{v} - \underline{v}_{ax} \tag{2}$$

The secondary velocity is in the plane of the slice it can be further decomposed into two components. Given the circular cross-section switching to a polar coordinate-system around the centreline point $\underline{r}_c$ is beneficial. So the secondary velocity can be decomposed into a radial and a circumferential component. First a radial unit vector is calculated using Eq. (3) between $\underline{r}_c$ and an arbitrary point p in the slice. Using the radial unit vector the radial component, $\underline{v}_{rad}$ of the secondary velocity can be calculated as seen in Eq. (4). The circumferential velocity $\underline{v}_{cir}$ can be calculated by simply subtracting the radial velocity from the secondary velocity as seen in Eq. (5). [11]

$$\underline{r}_{rad} = \frac{\underline{p} - \underline{r}_c}{\left|\underline{p} - \underline{r}_c\right|} \tag{3}$$

$$\underline{v}_{rad} = (\underline{v}_{sec} \cdot \underline{r}_{rad}) \cdot \underline{r}_{rad} \tag{4}$$

$$\underline{v}_{cir} = \underline{v}_{sec} - \underline{v}_{rad} \tag{5}$$

After computing the various velocity components in the slices, the average of each was computed for each slice along the centreline.

4. RESULTS

In the following section the findings will be explained, based on velocity graphs along the centreline between different configurations.

As the length of the centreline varies considerably between different configurations, it was made dimensionless for the graphs. The straight sections of the pipe were made dimensionless with the diameter. For the bend sections the length of the arc was chosen, which is the quarter circle. The reference point was set to the halfway point between the two pipe bends, shown in blue in Fig 1. So negative values along the x-axis are towards the inlet, and positive values are towards the outlet. The inlet straight section is not shown on the graphs to help with readability. The velocity component magnitude averages were normalized with the average of the inlet velocity.

The first grouping was done by fixing the diameter and the value of x_1 and changing the value of the curvature of the pipe bends. For $D = 4\,mm, x_1 = 0,\ Re = 100$ the results can be seen in Figs. 2., 3.

As R/D decreases, the maximum value of the circumferential velocity increases in both bends.

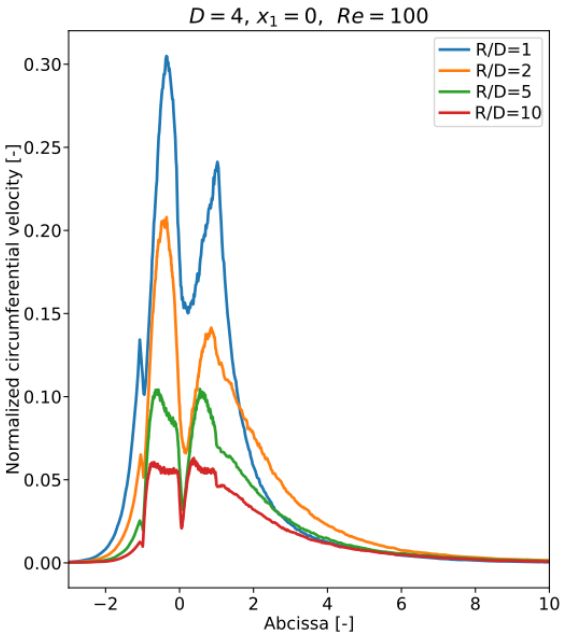

Figure 2. Plot of the circumferential velocity for $D = 4\ mm, x_1 = 0,\ Re = 100$

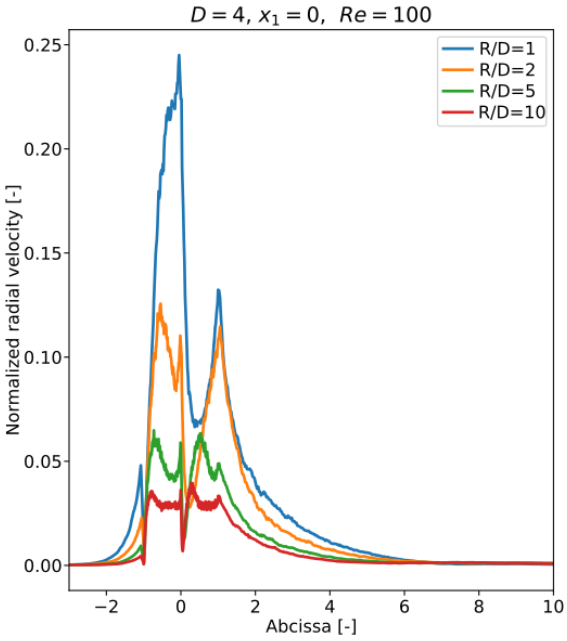

Figure 3. Plot of the radial velocity for $D = 4\ mm, x_1 = 0,\ Re = 100$

This is because a higher R/D ratio means the bend is shallower. An infinitely high ratio would mean straight pipe, where no circumferential velocity would develop. The local maxima in the second bend are lower than in the first bend for $R/D = 1$ and $R/D = 2$. For the other two configurations the maxima in the two bends are equal. With the exception of $R/D = 10$, the velocity in both bends have distinct maximum, while $R/D = 10$ has the shape of a plateau. In the second bend the location of the maximum moves towards the end of the bend as R/D decreases. The circumferential velocity dissipates faster for $R/D = 1$, as in the other cases, while having the highest maximum in the second bend.

The radial velocity graph shows similar findings to the circumferential ones. $R/D = 1$ and $R/D = 2$ have lower local maximum values in the second bend, though the values are similar despite the difference in the maxima in the first bend. The local maxima are further towards the end of the bends in both bends. For $R/D = 2$ and $R/D = 5$ a secondary rise can be seen at the end of the first bend. This rise in radial velocity also appears in the second bend for $R/D = 5$ with a lower value than in the first bend. After the second bend the radial velocity decreases in a similar manner for all the different R/D ratios.

With the increase of the Reynolds-number to 800 both graphs change considerably. The graph for the circumferential velocity can be seen in Fig. 4. and Fig. 5. The maxima are higher than in the case of $Re = 100$, meaning that relative importance of the secondary flows is higher than in the case of the lower Reynolds number.

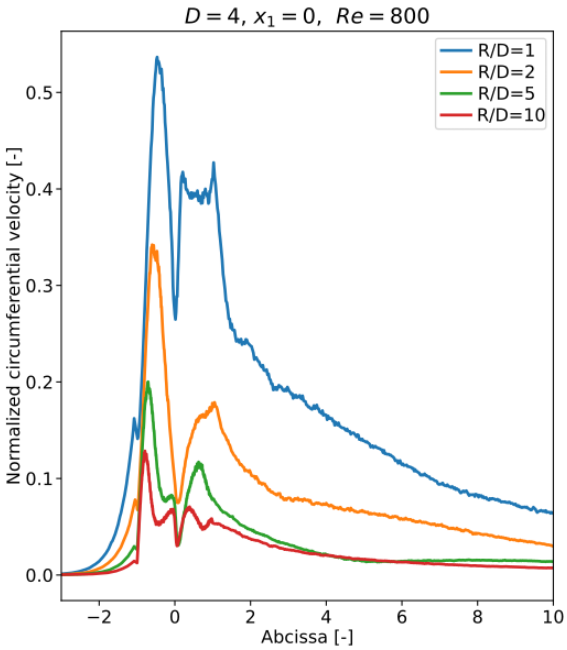

Figure 4. Plot of the circumferential velocity for $D = 4\ mm, x_1 = 0,\ Re = 800$

As for the second bend, the local maxima are smaller than in the first bend for all configurations.

The dissipation of the circumferential velocity takes longer and differs more between the different R/D ratios. The longer dissipation is probably caused by the higher relative velocity values.

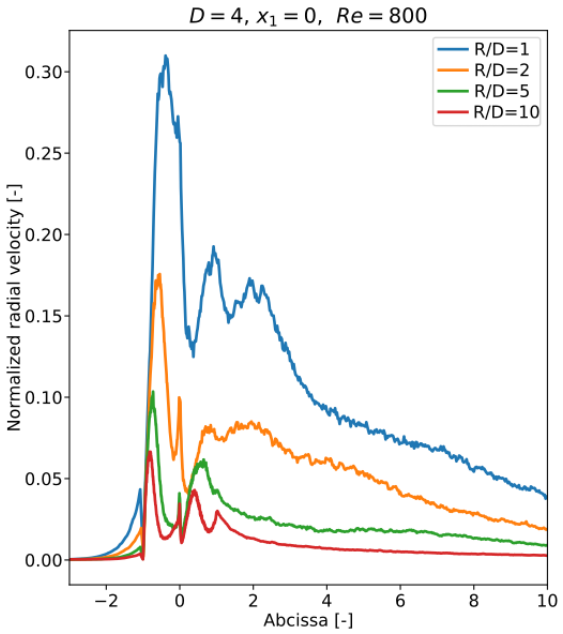

Figure 5. Plot of the radial velocity for $D = 4\ mm, x_1 = 0,\ Re = 800$

The plot of the radial velocity shows the radial velocity in comparable range to Fig. 3. This is in contrast with the circumferential velocity, where with the increase of the Reynolds number the relative velocity increased. The maximum in the first bend moves backwards as the R/D ratio decreases, and the increases as R/D decreases. In the second bend the local maxima are lower than in the first bend for all configurations. After the second bend increases in the radial velocity can be observed for $R/D = 1$ and $R/D = 2$

The effect of the length of the straight section was also investigated. The results will be shown for $R/D = 5$, as it is the shows the trends the best. The first graph in Fig. 6. shows the circumferential velocity for $Re = 100$. The graphs show identical trends in the two bends and between each other too. Also visible is that with the increase of x_1 the minimum value between the two bends decreases. The radial velocity graph seen in Fig. 7. shows similar results to Fig 6. The trends look nearly identical between the different configurations and between each other. As expected, the minimum between the bends decreases as x_1 increases. The difference is that the radial velocity graphs have a secondary peak in each bend.

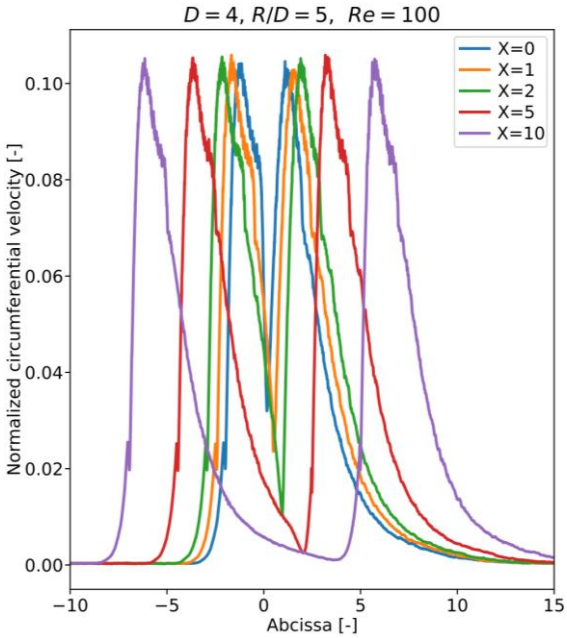

Figure 6. Plot of the circumferential velocity for $D = 4\ mm,\ R/D = 5,\ Re = 100$

For $Re = 800$ the circumferential velocity graph is shown in Fig. 8. The results for the first bend show matching shapes for each configuration. The minimum between the bends decreases as x_1 increases, as seen in the case of $Re = 100$. The results for the second differ though. The maxima are lower than in the first bend. It also increases as x_1 increases. The relative velocity maxima is two times higher than in the case of $Re = 100$.

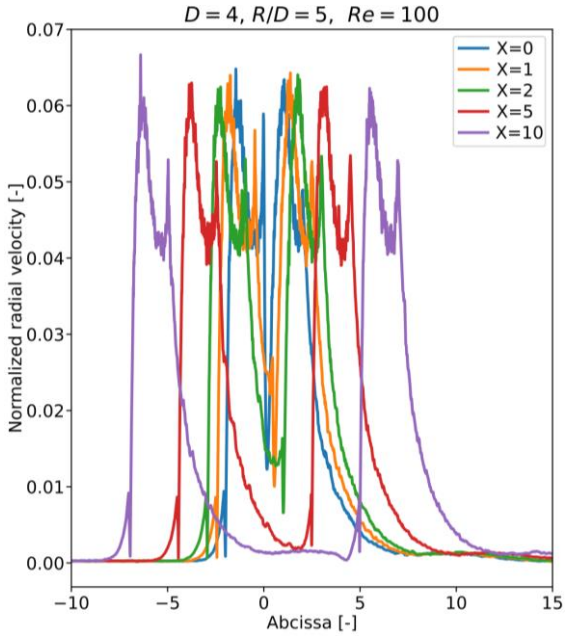

Figure 7. Plot of the radial velocity for $D = 4\ mm,\ R/D = 5,\ Re = 100$

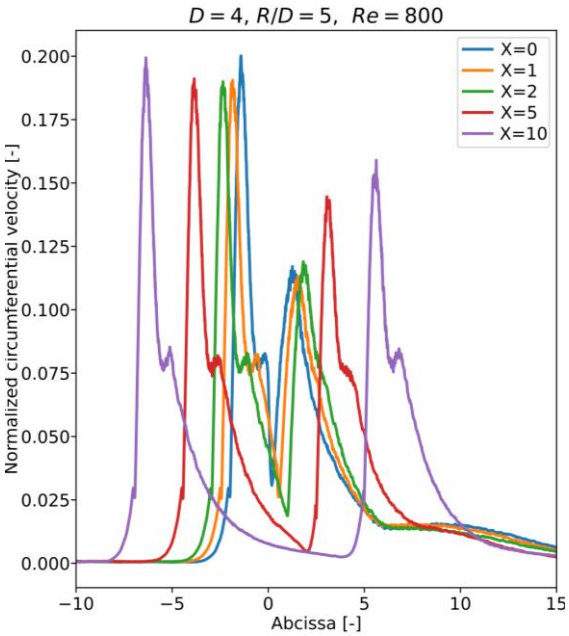

Figure 8. Plot of the circumferential velocity for $D = 4\ mm,\ R/D = 5,\ Re = 800$

The results for the radial velocity can be seen in Fig. 9. The results show similarities to both Fig 8. and Fig. 7. The shape of the graphs for the first bend are nearly identical. The minimum between the bends decreases as x_1 increases. The maxima in the second bend are again lower, than in the first bend, and increases as x_1 increases. The range is again similar to the case of $Re = 100$ and thus lower than the range of the circumferential velocity.

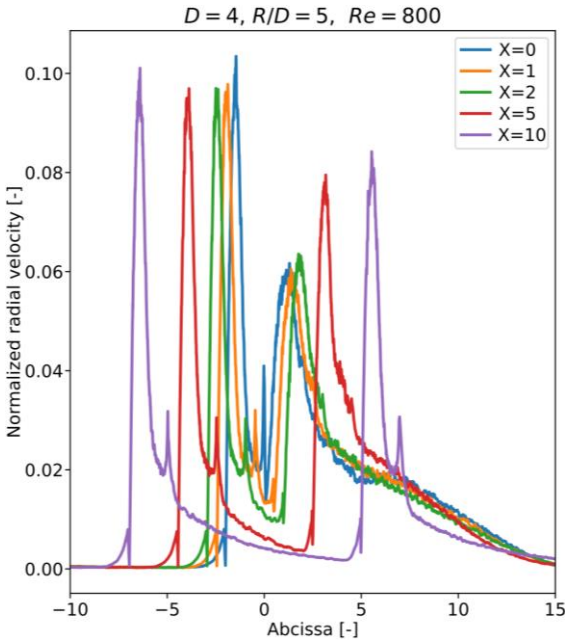

Figure 9. Plot of the radial velocity for $D = 4\ mm,\ R/D = 5,\ Re = 800$

However, the shapes between the first and second bend do not look as similar as in Fig. 7. The exception is $x_1 = 10$. The second rise up in velocity is not present in the second bend.

5. SUMMARY

The goal of the paper was to explore the effects of two pipe bends in opposite directions on secondary flows. A simple geometry was created which consisted of two 90° pipe bends with a straight section between them. It had three parameters which were changed. The flow was studied by steady state CFD simulations at different Reynolds-numbers. All the parameters were chosen to reflect real morphological data, to support research regarding the effect secondary flows on cardiovascular diseases.

At low Reynolds-number the first bend has less effect on the second one in most configurations. The exceptions for both in terms of radial and circumferential velocity happen when $x_1 = 0$ and the bends have a radius of $R/D = 1$ and $R/D = 2$. In these cases, the maximum values were lower than in the first bend. The radial and circumferential velocities were in the same range. At $Re = 800$ the first bend affected the developed flow noticeably. The local maxima in the second bend were smaller than in the first bend. This effect was stronger when x_1 was small. As x_1 increased the maxima in the second bend increased. As the bends were in opposite directions, they induce vortices in opposing rotating directions. So, the second bend first must slow down the vortices from the first bend and then starts to induce vortices in the opposite direction, hence the lower maximum values. Increasing the distance between the bends allows the secondary flows to dissipate more, thus the second bend can induce faster secondary flows. But even with the distance of 10 diameters, the maxima for both secondary velocity components were lower than in the first bend. With the increase of the Reynolds-number and in turn the velocity, the relative circumferential velocity increased considerably more than the relative radial velocity. The relative radius of R/D affected the location of the maximum secondary velocity location inside the bend.

In conclusion the first bend has a significant effect on the flow in the second bend, particularly at higher Reynolds-numbers. The distance between the bends also plays a crucial role in the strength of secondary flows in the second bend. The relative radius affects both the strength of the secondary flows and the location of the maxima inside the bend. These findings have implications for understanding the development of cardiovascular diseases, particularly in relation to aneurysm formation. The exact location of the secondary flow maximum is of interest as elevated secondary flows show correlation with aneurysm formation. [12]

The research can be extended to include more configurations, like non-planar cases or bends with non-constant radius. The effect of oscillatory and pulsatile flow may also be worth considering.

ACKNOWLEDGEMENTS

The project supported by the Doctoral Excellence Fellowship Programme (DCEP) is funded by the National Research Development and Innovation Fund of the Ministry of Culture and Innovation of Hungary and the Budapest University of Technology and Economics

Péter Friedrich and his work were supported by the Gedeon Richter Talentum Foundation in the framework of the Gedeon Richter Excellence PhD Scholarship

REFERENCES

[1] A. Lauric, J. Hippelheuser, M. G. Safain, and A. M. Malek, "Curvature effect on hemodynamic conditions at the inner bend of the carotid siphon and its relation to aneurysm formation," J Biomech, vol. 47, no. 12, pp. 3018–3027, Sep. 2014, doi: 10.1016/j.jbiomech.2014.06.042.

[2] B. Csippa, G. Závodszky, G. Paál, and I. Szikora, "A new hypothesis on the role of vessel topology in cerebral aneurysm initiation," *Comput Biol Med*, vol. 103, no. June, pp. 244–251, Dec. 2018, doi: 10.1016/j.compbiomed.2018.10.018.

[3] W. R. Dean, "XVI. Note on the motion of fluid in a curved pipe," *The London, Edinburgh, and Dublin Philosophical Magazine and Journal of Science*, vol. 4, no. 20, pp. 208–223, Jul. 1927, doi: 10.1080/14786440708564324.

[4] F. T. Smith, "Pulsatile flow in curved pipes," 1975.

[5] C. C. Hamakiotes and S. A. Berger, "Fully developed pulsatile flow in a curved pipe," 1988.

[6] K. Yamamoto ', S. Yanase, and T. Yoshida, "lirilii P Torsion effect on the flow in a helical pipe," 1994.

[7] D. G. Xie, "Torsion effect on secondary flow in helical pipe."

[8] "Steady flow in a helically symmetric pipe," 1998.

[9] "Unsteady blood flow in a helically symmetric pipe," 1998.

[10] M. R. Najjari and M. W. Plesniak, "Secondary flow vortical structures in a 180 elastic curved vessel with torsion under steady and pulsatile inflow conditions," *Phys Rev Fluids*, vol. 3, no. 1, Jan. 2018, doi: 10.1103/PhysRevFluids.3.013101.

[11] B. Csippa, L. Sándor, and G. Paál, "Decomposition of velocity field along a centerline curve using frenet-frames: Application to arterial blood flow simulations," *Periodica Polytechnica Mechanical Engineering*, vol. 65, no. 4, pp. 374–384, 2021, doi: 10.3311/PPME.18517.

[12] B. Csippa, P. Friedrich, I. Szikora, and G. Paál, "Amplification of Secondary Flow at the Initiation Site of Intracranial Sidewall Aneurysms," *Cardiovasc Eng Technol*, 2025, doi: 10.1007/s13239-025-00771-4.